THE ASTROPHYSICAL JOURNAL, 529:952–960, 2000 February 1

EVIDENCE FOR DOPPLER-SHIFTED IRON EMISSION LINES IN BLACK HOLE CANDIDATE 4U 1630−47

WEI CUI,[1] WAN CHEN,[2,3] AND SHUANG NAN ZHANG[4]
Received 1999 June 18; accepted 1999 September 21

ABSTRACT

We report the first detection of a pair of correlated emission lines in the X-ray spectrum of black hole candidate 4U 1630−47 during its 1996 outburst, based on *Rossi X-Ray Timing Explorer* (*RXTE*) observations of the source. At the peak plateau of the outburst, the emission lines are detected, centered mostly at ∼5.7 and ∼7.7 keV, respectively, while the line energies exhibit random variability ∼5%. Interestingly, the lines move in a concerted manner to keep their separation roughly constant. The lines also vary greatly in strength, but with the lower energy line always much stronger than the higher energy one. The measured equivalent width ranges from ∼50 to ∼270 eV for the former, and from insignificant detection to ∼140 eV for the latter; the two are reasonably correlated.

The correlation between the lines implies a causal connection; perhaps they share a common origin. Both lines may arise from a single Kα line of highly ionized iron that is Doppler shifted either in a Keplerian accretion disk or in a bipolar outflow or even both. In both scenarios, a change in the line energy might simply reflect a change in the ionization state of line-emitting matter. We discuss the implication of the results and also raise some questions about such interpretations.

Subject headings: binaries: general — line: profiles — stars: individual (4U 1630−47) — X-rays: stars

1. INTRODUCTION

Discovered by the *Uhuru* mission (Jones et al. 1976), 4U 1630−47 is a well-studied black hole candidate (BHC; Tanaka & Lewin 1995 and references therein; also see, e.g., Parmar, Angelini, & White 1995, Parmar et al. 1997, Kuulkers et al. 1997, and Oosterbroek et al. 1998 for more recent results). The source lies in the general direction of the Galactic center. Observations show that the source is heavily absorbed in soft X-rays, indicating a large distance (≳10 kpc) within the disk of our Galaxy. No optical counterpart has yet been identified, perhaps due to expected large visual extinction (>20 mag), so the dynamical evidence for the presence of a black hole in the binary system is still missing. 4U 1630−47 is considered a BHC only because of its similarities in the X-ray properties to some of the dynamically determined black hole systems (Parmar, Stella, & White 1986). It is a transient X-ray source, like most known BHCs, but is one of few such sources that exhibit frequent X-ray outbursts (e.g., Jones et al. 1976; Priedhorsky 1986; Kuulkers et al. 1997).

The canonical X-ray continuum of a BHC consists of two components (see review by Tanaka & Lewin 1995 and references therein): an ultrasoft component at low energies (<10 keV) and a power-law component at high energies, with photon indices roughly in the range of 1.5–2.5. The shape of the former is roughly that of a blackbody with temperature a few tenths to ∼2 keV, and has been successfully modeled by X-ray emission from the innermost portion of an optically thick (but geometrically thin) accretion disk surrounding the central black hole, while the latter is generally attributed to inverse Comptonization processes due to the presence of energetic electrons (thermal or nonthermal or both) in the binary system. For transient BHCs, the disk component dominates the overall X-ray energy output over the Compton component near the peak of an X-ray outburst (which is similar to the soft state for persistent BHCs like Cygnus X-1, in terms of the observed X-ray properties). Observations show that the power-law component is steep (with photon index ∼2.5) and extends to nearly 1 MeV without any apparent breaks (Grove et al. 1998), which would seem to signify the role of nonthermal Comptonization in the X-ray production processes (Coppi 1999 and references therein). As the outburst decays, the power-law component becomes flatter and thus increasingly dominant in the energy distribution; it also breaks at tens to several hundred keV, which is the signature of thermal Comptonization. The studies of 4U 1630−47 have shown that, for the most part, the source fits this description.

Emission lines, as well as absorption lines and edges, are sometimes observed in the X-ray spectrum of BHCs (e.g., Barr, White, & Page 1985; Kitamoto et al. 1990; Done et al. 1992; Ebisawa et al. 1996; Cui et al. 1997a, 1997b, 1998; Ueda et al. 1998). These narrow spectral features appear in the energy range 6–8 keV and are usually attributed to emission or absorption processes involving iron K-shell electrons. Although the exact location of line-emitting matter is often debatable, there is evidence, at least for some BHCs (e.g., Fabian et al. 1989; Cui et al. 1998; Życki, Done, & Smith 1999), that the observed iron Kα line originates in the innermost part of the accretion disk, close to the black hole. If this proves to be the case, the profile of such lines would be distorted by the strong gravitational field of the hole (e.g., Fabian et al. 1989) and could then be carefully modeled to possibly derive the intrinsic properties of the hole, such as its angular momentum (Laor 1991; Bromley, Chen, & Miller 1997). Also observed are Doppler-shifted emission lines from the relativistic jets of SS 433 (Kotani et al. 1996), which is sometimes thought to contain a neutron star, although this is highly debatable (Mirabel &

[1] Center for Space Research, Massachusetts Institute of Technology, Room 37-571, Cambridge, MA 02139; cui@space.mit.edu.

[2] NASA Goddard Space Flight Center, Code 661, Greenbelt, MD 20771; chen@milkyway.gsfc.nasa.gov.

[3] Also Department of Astronomy, University of Maryland, College Park, MD 20742.

[4] Physics Department, OB 428, University of Alabama in Huntsville, Huntsville, AL 35899; Shuang.Zhang@msfc.nasa.gov.

Rodríguez 1999). The studies of such lines have proved fruitful in gaining insights into the physical properties of the jets (Kotani et al. 1996). The emission lines could, therefore, become a valuable tool for probing the immediate surroundings of X-ray–emitting regions, in terms of their geometry and kinematics, and provide important diagnostics of matter there, such as its abundance and ionization state. In this paper, we report, for the first time, the detection of a pair of correlated emission lines in the X-ray spectrum of 4U 1630−47 during its 1996 outburst, using archival data from the *Rossi X-Ray Timing Explorer* (*RXTE*).

2. OBSERVATIONS

Figure 1 shows the light curve of 4U 1630−47, obtained by the All-Sky Monitor (ASM) aboard *RXTE*, that highlights the portion of its "flat-topped" 1996 X-ray outburst when the source was also observed by *RXTE*'s main instruments.[5] The 16 pointed *RXTE* observations (as marked in Fig. 1) cover a good portion of the peak plateau of the outburst, initially at a pace of once per day but at a much reduced pace toward the end of the monitoring campaign. The last observation occurred near the end of the decaying phase, about 2 months after the onset of the outburst. This particular observation has provided a valuable data set for studying the transition period as the source was on its way back to the quiescent state and for comparing the X-ray properties between a "low state" and a "high state" (i.e., during the peak of the outburst).

RXTE carries two pointing instruments, the Proportional Counter Array (PCA) and the High-Energy X-Ray Timing Experiment (HEXTE). The PCA covers a nominal energy range of 2–60 keV and the HEXTE 15–250 keV. Although our main focus in this study is on spectral lines, we have examined data from both instruments, hoping to better constrain the underlying continuum with a wider energy band. Unlike typical BHCs, however, the observed X-ray spectrum of 4U 1630−47 at the peak of the outburst is so steep (few PCA counts above ~30 keV) that the short HEXTE exposures provide little additional information. Hence, we present the results from analyzing only the PCA data. Table 1 summarizes the key parameters of the PCA observations. Note that the PCA consists of five individual Proportional Counter Units (PCUs), but not all PCUs were turned on during all observations.

[5] The full ASM light curve can be obtained from the public archival database maintained by the *RXTE* Guest Observer Facility through their web site at http://heasarc.gsfc.nasa.gov/docs/xte/asm_products.html.

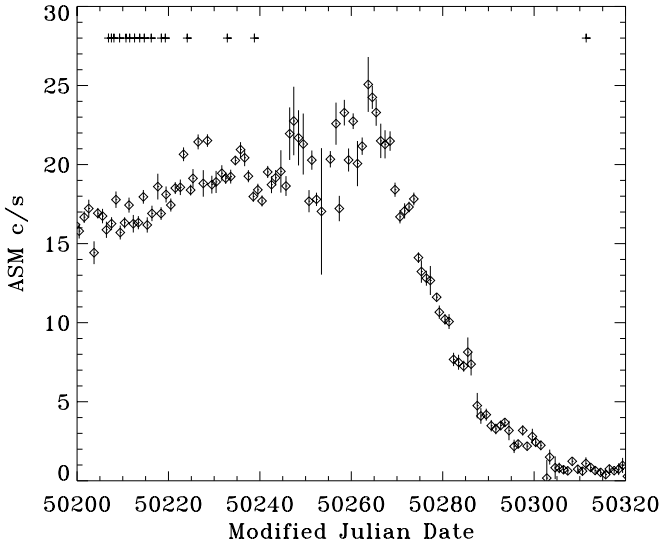

FIG. 1.—ASM light curve of 4U 1630−47 during its 1996 X-ray outburst. Each data point represents a 1 day averaged measurement. As a reference, the Crab produces about 75 Hz.The crosses at the top indicate the times of the pointed *RXTE* observations.

3. DATA ANALYSIS AND RESULTS

We performed spectral analysis using the *Standard 2* data. For all PCUs, the calibration of the first xenon layer has achieved the most satisfactory results, while that of the other two layers is more uncertain, especially in the energy

TABLE 1

PCA OBSERVATION LOG

Observation	Observation ID[a]	Date 1996	Observation Time (UT)	PCUs on	Exposure[b] (s)
1	02-00	May 3	20:37:00–22:40:00	5	2816[c]
2	03-00	May 4	12:11:00–14:03:00	5	3008
3	06-00	May 5	01:12:00–03:34:00	4	2368
4	04-00	May 6	06:59:00–09:39:00	4	3776
5	05-00	May 7	16:53:00–18:22:00	5	3536
6	01-00	May 8	11:48:00–13:03:00	4	2992
7	07-00	May 9	13:38:00–14:48:00	4	3488
8	08-00	May 10	16:33:00–17:59:00	3	3440
9	09-00	May 11	16:58:00–17:52:00	3	2784
10	11-00	May 13	05:39:00–08:08:00	3	4032
11	13-00	May 15	10:10:00–11:28:00	3	2976
12	14-00	May 16	07:16:00–08:27:00	3	2880
13	15-00	May 21	02:23:00–03:54:00	5	2320
14	16-00	May 29	21:03:00–23:10:00	5	4688
15	17-00	Jun 4	18:55:00–20:21:00	5	4064
16	18-00	Aug 16	08:51:00–09:19:00	5	1456

[a] With prefix 10411-01-.
[b] Total amount of on-source time after data filtering and screening.
[c] Excluding the period of dipping activity (~300 s).

range where iron spectral features are often observed. Therefore, we based our analysis on data from the first xenon layer only.

We used the calibration files (including response matrices and background models) delivered with the most recent release of FTOOLS (Version 4.2). For each observation, we constructed separate spectra (both source + background and background only) for the first layer of each PCU. We then carefully examined the quality of background models, under the assumption that the observed counts in the highest energy channels can be attributed entirely to the background. We found that the results were quite satisfactory except for two observations. In those two cases (observations 3 and 4 in Table 1), the background spectrum seems to be of the correct shape but the overall normalization is a bit too low. We have tried but failed to find any obvious culprits for the problem. For these two observations, we simply renormalized the background spectrum (by factors of 1.08 and 1.15, respectively) so that it matches the sum spectrum at the highest energy channels. This procedure seems to work well in the sense that the quality of background subtraction achieved for these two observations appears to be comparable to that for others. We also note that for observations 14 and 15, although the background spectrum looks reasonable on average, the individual data points scatter much more than usual at high energies. The cause for such excessive scatter is not clear either.

An important calibration issue is the lack of satisfactory estimation of the systematic uncertainties in the response matrices of the PCA. A common practice is to add a certain amount (e.g., 1% of total counts) in quadrature to Poisson errors uniformly across the entire energy range. We know that the uncertainty is significantly larger near xenon absorption edges, so this approach does not always work well for *RXTE* observations of bright sources, which are dominated by systematic uncertainties. In fact, this leads to a more fundamental problem about the applicability of the χ^2 statistics to the modeling of such *RXTE* data. While we can perhaps still use these statistics to compare different models to a certain degree, one should be cautious of relying on such statistics alone to reject or accept a certain model. Unfortunately, we are currently not aware of any more objective ways of estimating systematic uncertainties in the calibration of the PCA. Since our primary objective here is to study spectral lines, instead of modeling the continuum, we have decided to simply follow the common practice by adding 1% systematic error to the data. For this study, we are mostly concerned with the instrumental artifacts that are localized near the xenon edges, because they could mimic linelike features. For the first xenon layer, the known artifacts seem to be quite small.

After subtracting the background spectrum from the sum, we proceeded to model the resulting source spectrum. For the continuum, we adopted a composite model of a multicolor disk ("diskbb" in XSPEC; e.g., Mitsuda et al. 1984) and a power law, which is typical of BHCs. We then simultaneously applied the model to the first-layer spectra of all PCUs, with the relative (to PCU 0) normalization of the PCUs floating to account for any slight mismatches among the detectors. All the results are, therefore, normalized to the absolute calibration of PCU 0. This model alone fails to fit the observed X-ray spectrum in all cases (see the upper panel of Fig. 2 for observation 1); the residual plot

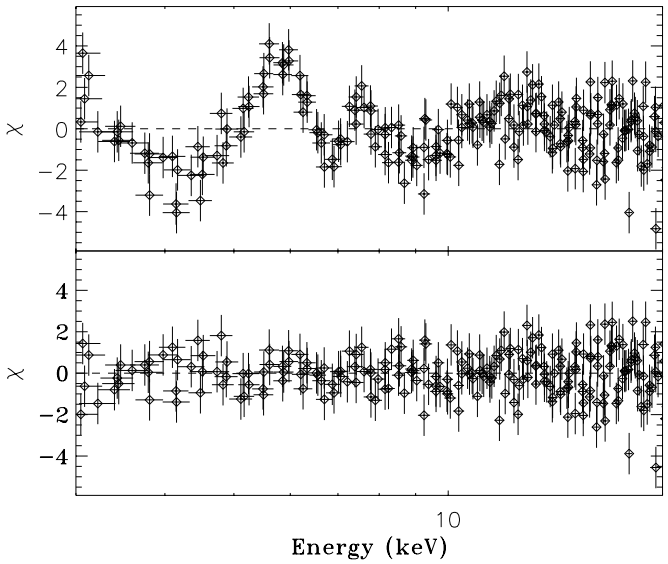

FIG. 2.—Nondip residual plots for observation 1. *Upper panel:* The continuum is modeled by a multicolor disk and a power law. *Lower panel:* The same continuum model plus two Gaussian functions.

reveals two linelike features between 5 and 8 keV. The fit becomes much improved (and formally acceptable in terms of the χ^2 statistics) after two Gaussian functions have been added to the model (see the lower panel of Fig. 2). Figure 3 shows the unfolded spectrum for observation 1, along with each individual component of the model. The lines are located at $\sim$5.5 keV and $\sim$7.5 keV, respectively, with equivalent widths $\sim$188 eV and $\sim$76 eV (see Table 3). We carried out the same analyses for other observations. The results are summarized in Tables 2 and 3 for the continuum and lines, respectively.

During the first observation, a large "dip" was observed in the X-ray intensity of the source, as shown in Figure 4. It has been suggested that the dip can be accounted for by a partial covering of the X-ray–emitting disk by some passing-by clouds, and that the complicated structures within the dip simply reflect the change in the absorbing

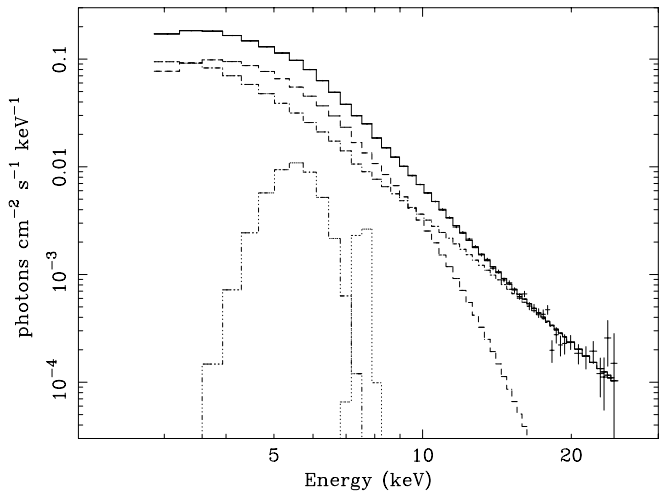

FIG. 3.—Unfolded X-ray spectrum for observation 1. For clarity, the spectra and model fits for individual PCUs have been co-added (for display only). Also shown is the contribution from each model component (see text for a description of the model adopted).

TABLE 2

X-RAY CONTINUUM[a]

OBSERVATION	N_H (10^{22} cm^{-2})	MULTICOLOR DISK[b] T_{dbb} (keV)	MULTICOLOR DISK[b] N_{dbb}	POWER LAW[c] α	POWER LAW[c] N_{pl}	χ^2_ν/dof
1	$11.5^{+0.6}_{-0.5}$	$1.26^{+0.01}_{-0.01}$	230^{+20}_{-20}	$4.06^{+0.11}_{-0.12}$	47^{+16}_{-14}	1.37/250
2	$10.5^{+0.4}_{-0.3}$	$1.249^{+0.005}_{-0.005}$	220^{+7}_{-8}	$3.79^{+0.10}_{-0.10}$	15^{+4}_{-4}	0.78/250
3	$10.6^{+0.5}_{-0.5}$	$1.250^{+0.005}_{-0.006}$	197^{+6}_{-7}	$3.89^{+0.13}_{-0.13}$	15^{+4}_{-4}	0.92/200
4	$14.1^{+0.5}_{-0.5}$	$1.31^{+0.01}_{-0.02}$	140^{+16}_{-15}	$4.77^{+0.08}_{-0.09}$	158^{+35}_{-32}	0.89/200
5	$13.1^{+0.6}_{-0.6}$	$1.316^{+0.008}_{-0.009}$	175^{+16}_{-18}	$4.47^{+0.10}_{-0.11}$	97^{+31}_{-24}	0.95/250
6	$11.5^{+0.5}_{-0.6}$	$1.336^{+0.006}_{-0.006}$	271^{+13}_{-11}	$4.19^{+0.10}_{-0.13}$	60^{+16}_{-18}	0.75/200
7	$15.1^{+0.6}_{-0.6}$	$1.40^{+0.03}_{-0.02}$	134^{+18}_{-15}	$5.04^{+0.09}_{-0.07}$	398^{+88}_{-70}	0.75/200
8	$15.8^{+0.7}_{-0.6}$	$1.38^{+0.03}_{-0.02}$	133^{+20}_{-20}	$4.97^{+0.10}_{-0.09}$	346^{+92}_{-75}	1.10/146
9	$13.8^{+0.5}_{-0.8}$	$1.32^{+0.01}_{-0.01}$	227^{+18}_{-15}	$4.65^{+0.09}_{-0.12}$	160^{+43}_{-46}	0.83/146
10[d]	$9.6^{+0.1}_{-0.1}$	$1.304^{+0.002}_{-0.003}$	236^{+2}_{-2}	$3.13^{+0.07}_{-0.08}$	$3.5^{+0.8}_{-0.7}$	4.44/146
11	$13.9^{+0.9}_{-0.6}$	$1.32^{+0.02}_{-0.01}$	178^{+14}_{-23}	$4.62^{+0.14}_{-0.09}$	134^{+50}_{-29}	0.74/146
12	$11.9^{+0.6}_{-0.6}$	$1.319^{+0.006}_{-0.005}$	298^{+12}_{-13}	$4.18^{+0.11}_{-0.13}$	61^{+23}_{-10}	0.72/146
13	$9.4^{+0.3}_{-0.1}$	$1.332^{+0.006}_{-0.005}$	255^{+5}_{-5}	$3.31^{+0.11}_{-0.11}$	6^{+2}_{-2}	0.82/250
14[d]	$9.25^{+0.09}_{-0.04}$	$1.340^{+0.002}_{-0.003}$	312^{+2}_{-2}	$2.92^{+0.07}_{-0.03}$	$3.0^{+0.6}_{-0.3}$	10.96/250
15[d]	$11.9^{+0.8}_{-0.5}$	$1.343^{+0.004}_{-0.004}$	272^{+7}_{-16}	$4.32^{+0.16}_{-0.09}$	76^{+42}_{-18}	2.16/250
16	$7.0^{+1.1}_{-0.9}$	$0.60^{+0.03}_{-0.02}$	765^{+463}_{-267}	$1.94^{+0.06}_{-0.06}$	$0.066^{+0.010}_{-0.008}$	0.74/253

[a] The uncertainties are derived by varying parameters until $\Delta\chi^2 = 1$. Hence, they correspond to 1 σ errors.

[b] T_{dbb} is the temperature of the inner edge of the disk, and the normalization N_{dbb} is defined as $(R_{dbb}/D)^2 \cos\theta$, where R_{dbb} is the radius of the inner edge of the disk in units of kilometers, D is the distance to the source in units of 10 kpc, and θ is the inclination angle of the disk.

[c] α is the photon index, and the normalization N_{pl} is defined as photon flux at 1 keV in units of photons cm^{-2} s^{-1} keV^{-1}.

[d] Note potential large systematic uncertainty in the measured continuum properties (see text)

column density through the clouds (Tomsick, Lapshov, & Kaaret 1998; see also Kuulkers et al. 1998). Although it is not our primary goal here to study the origin of the dip, for the purpose of comparison (the dip was excluded from the analysis already described), we constructed an average X-ray spectrum for the dip and conducted similar analyses with the same continuum model. We found that the dip spectrum can be described satisfactorily (in terms of the reduced χ^2 value) with the addition of only one Gaussian function (Fig. 5). The Gaussian seems to correspond to the lower energy line seen in the nondip spectrum, although the line seems much broader and stronger. The results for the dip are summarized in Table 4. In this model, no significant change is required in the line-of-sight column density during the dip (by comparing Table 4 with Table 2). Instead, *only* the disk component seems to have varied sig-

TABLE 3

DETECTED EMISSION LINES[a]

OBSERVATION	LOWER ENERGY LINE E_l (keV)	LOWER ENERGY LINE σ_l (keV)	LOWER ENERGY LINE EW$_l$ (eV)	HIGHER ENERGY LINE E_h (keV)	HIGHER ENERGY LINE σ_h (keV)	HIGHER ENERGY LINE EW_h (eV)	E_m[b] (keV)	ΔE[b] (keV)
1	$5.46^{+0.08}_{-0.09}$	$0.62^{+0.08}_{-0.09}$	188^{+42}_{-34}	$7.55^{+0.06}_{-0.07}$	$0.17^{+0.15}_{-0.17}$	76^{+14}_{-16}	$6.50^{+0.05}_{-0.06}$	$2.09^{+0.10}_{-0.11}$
2	$5.66^{+0.08}_{-0.10}$	$0.47^{+0.10}_{-0.10}$	94^{+22}_{-17}	$7.66^{+0.08}_{-0.07}$	$0.0^{+0.2}_{-0.0}$	36^{+8}_{-7}	$6.66^{+0.06}_{-0.06}$	$2.00^{+0.11}_{-0.12}$
3	$5.76^{+0.08}_{-0.08}$	$0.34^{+0.10}_{-0.12}$	75^{+17}_{-14}	$7.70^{+0.06}_{-0.12}$	$0.0^{+0.5}_{-0.0}$	27^{+12}_{-8}	$6.73^{+0.05}_{-0.07}$	$1.94^{+0.10}_{-0.14}$
4	$5.42^{+0.12}_{-0.14}$	$0.69^{+0.11}_{-0.11}$	169^{+53}_{-41}	$7.67^{+0.07}_{-0.07}$	$0.16^{+0.14}_{-0.16}$	73^{+18}_{-15}	$6.54^{+0.07}_{-0.08}$	$2.25^{+0.14}_{-0.16}$
5	$5.57^{+0.12}_{-0.14}$	$0.57^{+0.15}_{-0.13}$	121^{+26}_{-31}	$7.62^{+0.14}_{-0.20}$	$0.60^{+0.16}_{-0.15}$	93^{+43}_{-26}	$6.60^{+0.09}_{-0.12}$	$2.05^{+0.18}_{-0.24}$
6	$5.69^{+0.10}_{-0.11}$	$0.48^{+0.12}_{-0.12}$	85^{+24}_{-19}	$7.83^{+0.08}_{-0.09}$	$0.0^{+2.2}_{-0.0}$	35^{+11}_{-9}	$6.76^{+0.06}_{-0.07}$	$2.14^{+0.13}_{-0.14}$
7	$5.21^{+0.15}_{-0.19}$	$0.84^{+0.14}_{-0.12}$	273^{+92}_{-66}	$7.64^{+0.06}_{-0.08}$	$0.38^{+0.10}_{-0.08}$	140^{+19}_{-27}	$6.42^{+0.08}_{-0.10}$	$2.43^{+0.16}_{-0.21}$
8	$5.46^{+0.14}_{-0.17}$	$0.65^{+0.16}_{-0.13}$	162^{+70}_{-47}	$7.63^{+0.09}_{-0.06}$	$0.46^{+0.13}_{-0.17}$	131^{+50}_{-32}	$6.54^{+0.08}_{-0.09}$	$2.17^{+0.17}_{-0.18}$
9	$5.75^{+0.11}_{-0.12}$	$0.36^{+0.14}_{-0.18}$	64^{+22}_{-17}	$7.73^{+0.08}_{-0.09}$	$0.09^{+0.27}_{-0.09}$	46^{+19}_{-13}	$6.74^{+0.07}_{-0.08}$	$1.98^{+0.14}_{-0.15}$
10[c]	$5.79^{+0.02}_{-0.03}$	$0.31^{+0.04}_{-0.04}$	51^{+4}_{-4}	$7.80^{+0.08}_{-0.07}$	$0.0^{+0.1}_{-0.1}$	12^{+4}_{-2}	$6.80^{+0.04}_{-0.04}$	$2.01^{+0.08}_{-0.08}$
11	$5.63^{+0.11}_{-0.15}$	$0.48^{+0.16}_{-0.13}$	89^{+41}_{-24}	$7.65^{+0.08}_{-0.10}$	$0.18^{+0.24}_{-0.18}$	57^{+30}_{-15}	$6.64^{+0.07}_{-0.09}$	$2.02^{+0.14}_{-0.18}$
12	$5.78^{+0.10}_{-0.10}$	$0.25^{+0.14}_{-0.25}$	55^{+18}_{-13}	$7.76^{+0.11}_{-0.10}$	$0.0^{+0.3}_{-0.0}$	29^{+10}_{-9}	$6.77^{+0.07}_{-0.07}$	$1.98^{+0.15}_{-0.14}$
13	$5.78^{+0.08}_{-0.10}$	$0.21^{+0.13}_{-0.21}$	50^{+12}_{-10}	$7.85^{+0.22}_{-0.19}$	$0.0^{+0.3}_{-0.0}$	10^{+7}_{-6}	$6.82^{+0.12}_{-0.11}$	$2.07^{+0.23}_{-0.21}$
14[c]	$5.82^{+0.02}_{-0.01}$	$0.30^{+0.03}_{-0.03}$	54^{+3}_{-3}	$8.26^{+0.07}_{-0.11}$	$0.66^{+0.12}_{-0.11}$	29^{+11}_{-4}	$7.04^{+0.04}_{-0.06}$	$2.44^{+0.07}_{-0.11}$
15	$5.79^{+0.08}_{-0.03}$	$0.25^{+0.13}_{-0.17}$	50^{+17}_{-10}	$7.95^{+0.12}_{-0.19}$	$0.5^{+0.3}_{-0.2}$	46^{+19}_{-15}	$6.87^{+0.07}_{-0.10}$	$2.16^{+0.14}_{-0.19}$
16	$6.50^{+0.06}_{-0.08}$	$0.58^{+0.16}_{-0.11}$	453^{+131}_{-79}	–	–	–	$6.50^{+0.06}_{-0.08}$	–

[a] Listed properties include line energy, width (FWHM), and equivalent width (EW). The uncertainties correspond to 1 σ errors; see notes to Table 2.

[b] $E_m = (E_l + E_h)/2$; $\Delta E = E_h - E_l$.

[c] Note potential large systematic uncertainty in the measured line properties (see text).

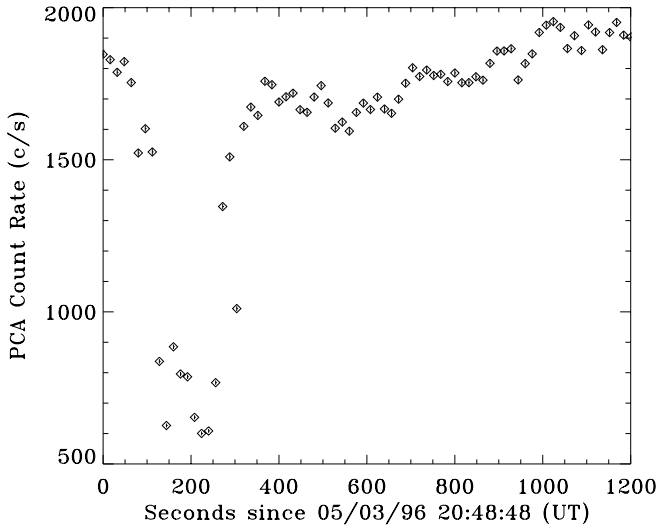

FIG. 4.—Light curve for observation 1. Note an intensity dip during the early part of the observation.

nificantly: the temperature at the inner edge of the disk becomes higher, but the overall normalization is lower, which perhaps indicates that the inner edge of the disk moves closer to the central black hole. This would be opposite to some of the dips observed in black hole candidate GRS 1915+105, which have been attributed to a viscous instability that causes the disruption of the inner part of the disk (Belloni et al. 1997). No similar dips are seen during the subsequent *RXTE* observations of 4U 1630−47.

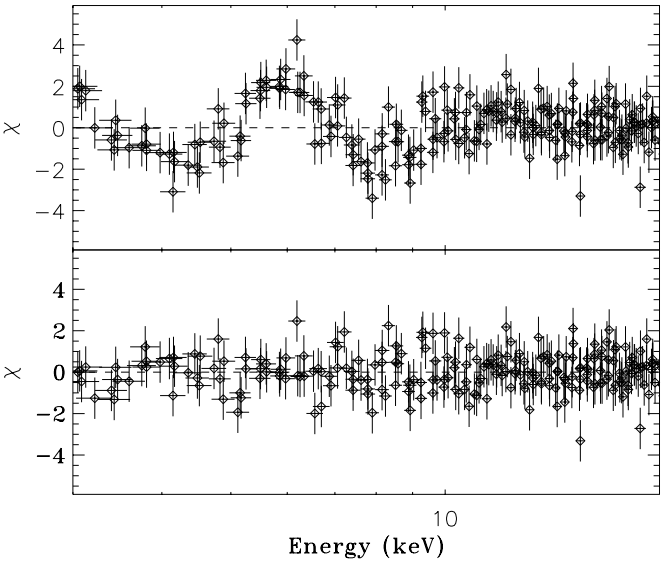

FIG. 5.—Same as Fig. 2, but for the dip. Note that only the lower energy line is apparent here.

It is clear, from Tables 2 and 3, that the model adopted seems to describe the observed X-ray spectra of 4U 1630−47 quite well, except for observations 10, 14, and 15. For observation 10, the large reduced χ^2 values are almost entirely due to significant structures in the residual at low energies (<10 keV); observation 14 suffers from the same problem, in addition to large residuals at high energies (>20 keV) that are caused by excessive scatter of data points in the background spectrum already mentioned; the latter also explains the problem for observation 15. These problems are illustrated in Figure 6, taking observation 14 as an example. The magnitude of the low-energy structures in observations 10 and 14 are quite small, compared with the emission lines detected. While the features might represent interesting real effects, we will not pursue them any further in this study.

The continuum of 4U 1630−47 is unusually soft during the peak of the 1996 outburst, with power-law photon indices in the range of 3–5 (for comparison, the photon index is typically around 2.5 for BHCs). The power-law component varies significantly during the outburst. The disk component appears quite typical of BHCs, with the temperature ∼1.3 keV at the inner edge of the disk. The high line-of-sight column density may simply indicate the location of the source: it is buried in the disk of our Galaxy and far away from us, as also concluded from other studies.

Although a pair of emission lines are detected in all observations during the peak of the outburst (the first 15 in Table 1), in some cases, the higher energy line is quite weak and thus the detection is not very significant. For such cases, the derived line equivalent width can be significantly affected by the calibration uncertainties. It is clear, however, that the detected lines cannot be entirely attributed to instrumental artifacts, because they vary greatly from observation to observation and show no apparent correlation with the exposure time (which roughly determines the signal-to-noise ratio of the data here). To further investigate possible artifacts caused by calibration uncertainties, we analyzed a PCA observation of the Crab (observation ID 10200-01-20-00) which was made during the same epoch (on 1997 January 13), following exactly the same procedure (e.g., only the first xenon layer of each PCU is used). The X-ray spectrum is well described by an absorbed power law, and the derived model parameters are all within the nominal values for the source ($N_{\rm H} = 3.1 \times 10^{21}$ cm^{-2}, photon index 2.16, and normalization 12.5 photons keV^{-1} cm^{-2} s^{-1}). The residuals of the fit can be quantified by the ratio of the data to the model. We obtained such residual plots for both the Crab and 4U 1630−47 (from the continuum model without Gaussian functions), and the ratio between the two plots should

TABLE 4

AVERAGE "DIP" SPECTRUM[a]

	MULTICOLOR DISK		POWER LAW		EMISSION LINE			
$N_{\rm H}$ (10^{22} cm^{-2})	$T_{\rm dbb}$ (keV)	$N_{\rm dbb}$	α	$N_{\rm pl}$	E (keV)	σ (keV)	EW (eV)	χ^2_ν/dof
$10.9^{+0.9}_{-1.2}$	$1.50^{+0.27}_{-0.18}$	18^{+33}_{-12}	$4.21^{+0.19}_{-0.23}$	48^{+23}_{-21}	$5.15^{+0.29}_{-0.33}$	$1.1^{+0.1}_{-0.2}$	620^{+383}_{-243}	0.84/253

[a] See Tables 2 and 3 for the definitions and units of the listed quantities. The uncertainties again correspond to 1 σ errors.

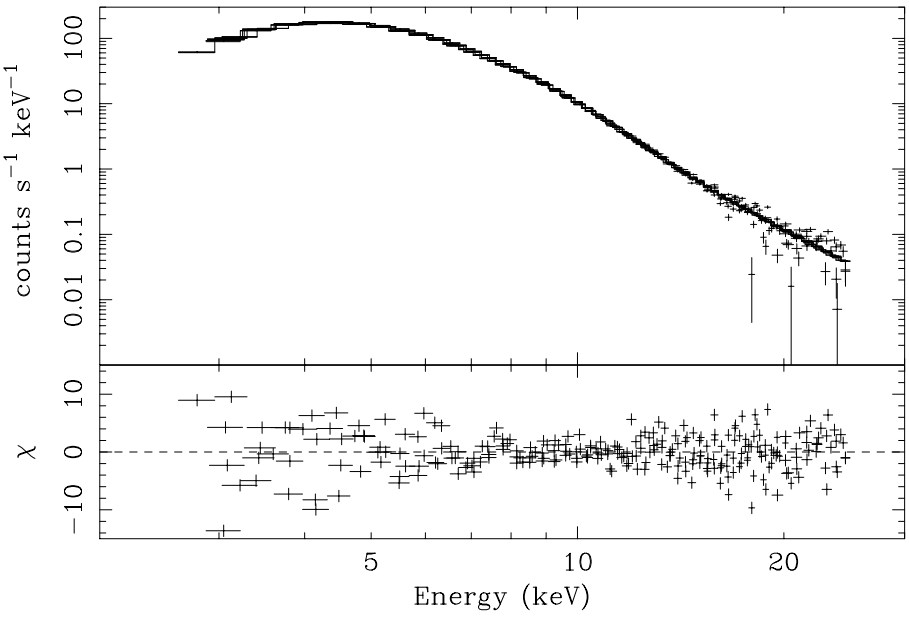

FIG. 6.—Measured X-ray spectrum from observation 14. The solid histogram shows the best-fit model, and the residuals of the fit are shown in the lower panel. Note large residuals at low and high energies.

roughly be free of any calibration uncertainties. One such ratio plot (for PCU 0 alone) is shown in Figure 7. The two emission lines are clearly present. Assuming that the spectrum of the Crab is featureless, we conclude that both lines are physically associated with 4U 1630−47, even though the inferred line parameters (physical width and equivalent width, in particular) may be sensitive to calibration uncertainties. Figure 8 highlights the detected emission lines in all observations after the underlying continuum has been subtracted from the source spectrum.

Only one emission line is present in the last observation (No. 16, as listed in Table 1; see also Fig. 8), as the source is just about to return to the quiescent state. Interestingly, the line is located roughly midway between the pair of lines seen during the peak of the outburst, and it appears to be much stronger. The measured power-law photon index ($\sim$2) is typical of transitional periods between "high" and "low" spectral states in BHCs (e.g., Cui et al. 1997a, 1997b). The X-ray–emitting portion of the disk seems to be much cooler, and the inner disk edge becomes farther away from the central black hole. The measured column density is $\sim$30% lower than that during the peak. Similar evolution of the column density was also noted in another study of 4U 1630−47 during the decaying phase of its 1998 outburst (Oosterbroek et al. 1999). It was speculated that a substantial amount of material could be produced at the onset of the outburst, which, subsequently, is either accreted onto the black hole or expelled from the binary system. Alternatively, the larger column density might indicate a significant increase in the scale height of the accretion disk during the outburst, if the binary system is highly inclined with respect to the line of sight (as speculated by Kuulkers et al. 1998).

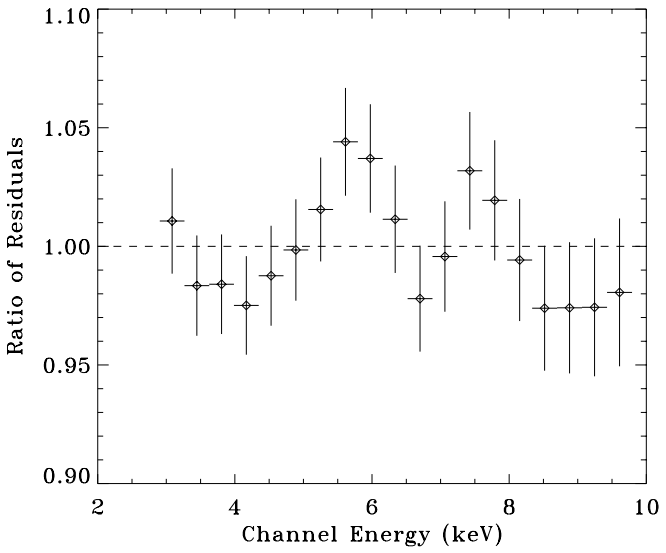

FIG. 7.—Ratio of the residual plot of 4U 1630−47 to that of the Crab. The residual plot is obtained by taking the ratio of the data (from the first xenon layer of PCU 0 only) to the model. For 4U 1630−47 the data are from observation 1, and the model consists of a multicolor disk and a power law (with absorption); for the Crab the model is an absorbed power law.

4. DISCUSSION

The *RXTE* observations of 4U 1630−47 have revealed the presence of two emission lines when the source was near the peak of its 1996 X-ray outburst. Although the lines seem to move around at random, they move in unison, so as to keep their separation roughly constant (see Table 3). Also, the lines vary significantly in strength, but with the lower energy line always much stronger than the higher energy one. The measured line fluxes are reasonably correlated, as shown in Figure 9. The correlation between the lines seems to imply a causal connection; perhaps they share a common origin. Probably, both originate in a single Kα line from highly ionized iron that is Doppler shifted either in a Keplerian accretion disk or in a bipolar outflow or even both. The required line-of-sight velocity is only roughly 0.15c, which can easily be accommodated in both scenarios. Although the detailed line properties (such as profiles) are expected to be different for the two cases, the lack of ade-

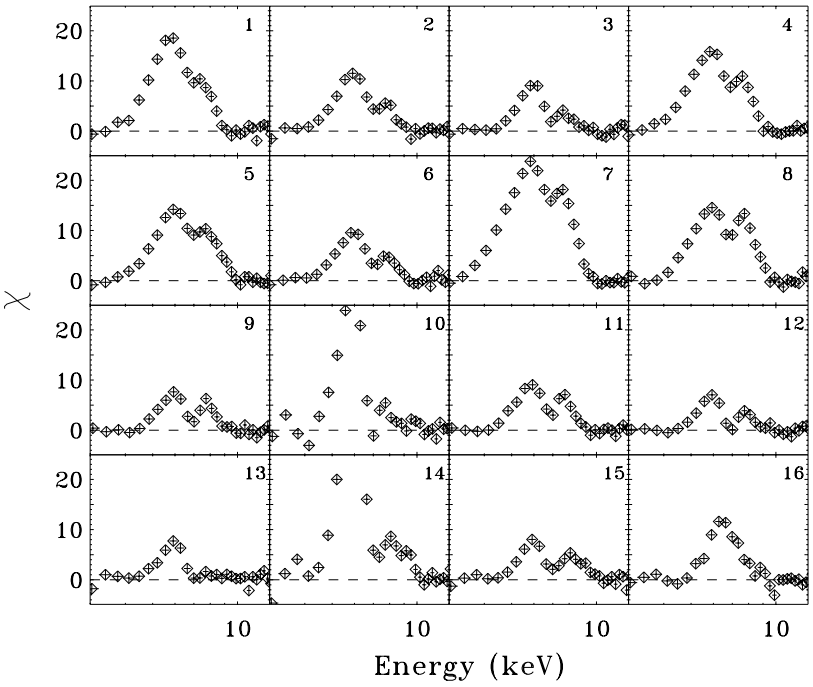

FIG. 8.—Detected emission lines. Each panel, labeled by the observation number, shows a residual plot after the underlying continuum is subtracted from the source spectrum. As in Fig. 3, individual PCU spectra have been co-added. Note potential large systematic uncertainty in observations 10 and 14 (see text).

quate energy resolution of the data makes it impossible to favor one over the other at present. In both cases, a change in the line energy might be due to the variation in the ionization state of the line-emitting matter.

If the observed emission-line pair is from a single, double-peaked iron Kα line that originates in the accretion disk close to the central black hole, both gravitational and transverse Doppler shifts would tend to move line photons toward lower energies. In this case, a stronger red peak may only reflect the skewness of the line profile, which is not resolved here, again because of the lack of energy resolution. Further support for a disk origin of the line pair can be derived from the fact that the higher energy line appears to be much narrower than the lower energy one in most cases (see Table 3). This favors a line profile with a much more extended red wing (than the blue wing), which is characteristic of a disk line. Moreover, during the dip, the inner edge of the disk appears to have moved closer to the black hole (see discussion in § 3). We would therefore expect that the red peak grows stronger, as a result of stronger gravitational redshift; this indeed appears to be the case (see Table 4). For a disk line, the highly blueshifted peak would necessarily require a rather high inclination angle of the accretion disk (e.g,, Fabian et al. 1989), which could be consistent with the observed dipping activity of 4U 1630−47 if the dip is caused by absorption (see arguments by Kuulkers et al. 1998). The presence of broad (or "smeared") iron lines from the accretion disk of other BHCs has previously been suggested by Życki and his coworkers in a series of papers (e.g., Życki et al. 1999 and references therein), by modeling the reflection component of the X-ray spectrum.

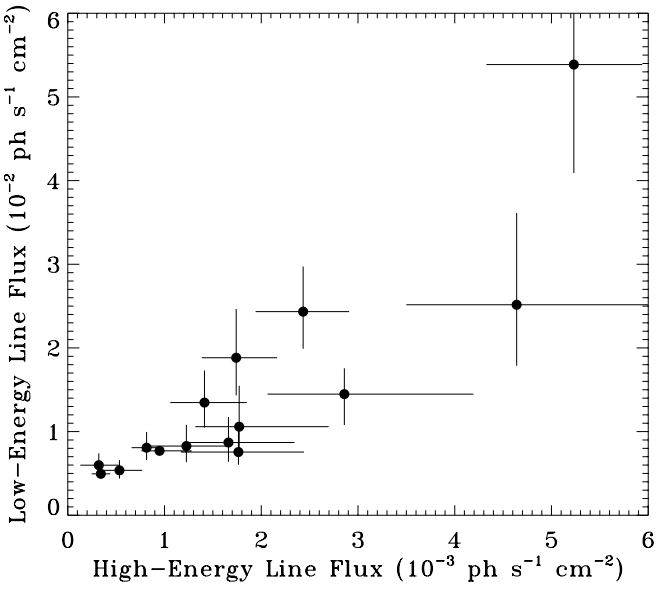

FIG. 9.—Correlation between the fluxes of the two emission lines. Note that the error bars are likely underestimated at low fluxes, due to remaining systematic uncertainties.

The outflow model, on the other hand, cannot naturally explain why the redshifted line is so much stronger than the blueshifted one, since the opposite is expected as the result of Doppler boosting. However, the problem is not fatal, because of our ignorance of astrophysical jets and the physical processes therein. It is known that the measured radio fluxes from the receding and approaching jets in "microquasars" are not always consistent with Doppler boosting (Hjellming & Rupen 1995; Fender et al. 1999). In fact, the receding jet sometimes appears brighter than the approaching one. Sometimes, the relative brightness of twin jets flip-flops as the jets evolve (see Fig. 2 in Fender et al. 1999). These "anomalies" almost certainly reflect the intrinsic difference between the two jets. Similar differences could also have existed in a bipolar outflow from 4U 1630−47, to

account for the observed line flux ratio. Moreover, the asymmetry in the environment surrounding either side of the outflow might cause, for example, the emission from the approaching flow being obscured more than that from the receding one, independent of any other physical processes. Therefore, the outflow scenario is by no means ruled out, although a disk origin of the observed emission lines does seem more likely.

Only one emission line is seen during the transition of the source to the quiescent state. For a line that originates in the innermost portion of the accretion disk, it would imply that the inner edge of the disk has moved farther away from the black hole (and thus the effects of Doppler shift become small) as the transition proceeded, consistent with the inferred evolution of the disk from the model fit (see § 3). It is worth pointing out that such evolution of the accretion disk agrees qualitatively with the expectation of the "advection-dominated accretion flow" (ADAF) models for state transitions in BHCs (e.g., Esin, McClintock, & Ramesh 1998). If the line originates in a bipolar outflow, on the other hand, a single-peaked line would imply that the velocity of the outflow is much reduced during the transition. Given the limited spectral resolution of the PCA, it is also possible that the observed lines are a mixture of emission lines both from the inner region of the accretion disk and from a bipolar outflow that might only occur during the peak of the outburst. In this case, the evolution of the emission line from being double-peaked to being single-peaked, as the source approaches the quiescent state, could be attributed to the cessation of the outflow and the receding of the inner edge of the accretion disk during the process. During the transition, the increase in the equivalent width of the line (see Table 3) is probably due to the combination of a much flatter power-law component and a larger solid angle subtended by a larger Comptonizing region (as required, e.g., by the ADAF models).

It is interesting that no emission lines of 4U 1630−47 have ever been reported previously. This can be attributed either to the much improved spectral capability of the *RXTE* instrumentation, especially the large effective area of the PCA, which is essential for detecting relatively weak, broad lines, or to the rare occurrence of such spectral features. Indeed, the observed X-ray properties of 4U 1630−47 during the 1996 outburst appear to be somewhat unusual, compared to other transient BHCs in outburst. Most notably, the observed X-ray continuum is extremely soft: hardly any counts are detected above ~ 30 keV. At high energies, the continuum can still be well described by a single power law but the photon index reaches as high as ~ 5, compared to typical values of less than 3 for BHCs. In 1998, 4U 1630−47 experienced another X-ray outburst, which was well covered by the ASM/*RXTE*,[6] as well as by the *RXTE*'s pointing instruments. We will report the results for this outburst in a future publication (Cui et al. 2000, in preparation). The preliminary spectral results from the PCA data give no indication for the presence of a similar emission-line pair during the outburst. The observed power-law continuum is quite typical of BHCs, which was also noted based on the results from *BeppoSAX* observations (Oosterbroek et al. 1998). Perhaps, the 1996 outburst is an unusual one for 4U 1630−47, in which a bipolar outflow might indeed have been formed. The source was observed at radio wavelengths with the Australia Telescope Compact Array and the Very Large Array during this period, but no emission was detected (Kuulkers et al. 1997; Hjellming et al. 1999, although radio emission was observed during the 1998 outburst, which the authors suggested as evidence for the presence of jets).

Finally, it seems reasonable to ask why no Doppler-shifted emission lines have ever been observed of the "microquasars" that are known to occasionally produce relativistic bipolar jets with superluminal motion, if the observed pair of emission lines might indicate the formation of bipolar outflows in 4U 1630−47 during the peak of its 1996 outburst. Insufficient coverage at X-rays is unlikely to be the answer, since at least in the case of GRS 1915+105 the source was regularly monitored by *RXTE* during a period when superluminal radio jets were detected (Fender et al. 1999). In fact, the observations of GRS 1915+105 at other times provided evidence for more subtle mass ejection events, combined with observations at other wavelengths (Eikenberry et al. 1998; Mirabel et al. 1998), yet no Doppler-shifted X-ray lines were reported. Either such lines were overlooked in the published work based on these observations, or they were simply not present. We think that the latter is more likely, especially considering the fact that no reliable detection has been reported of any emission lines in microquasars. It has been speculated that the general lack (or the weakness) of iron Kα lines in BHCs can be attributed to the high ionization state of matter in the vicinity of central black holes due to relatively high X-ray luminosity (Ross & Fabian 1993; Matt, Fabian, & Ross 1996). It is known that the fluorescent photons from Fe XVII–Fe XXIII are very likely to be resonantly absorbed by the next ionized species and eventually destroyed by the Auger effect in a typical environment such as an accretion disk (Ross & Fabian 1993). Consequently, no (or very weak) iron Kα lines are expected. At even higher ionization states, however, the Kα lines from Fe XXIV–Fe XXVI can escape rather easily, due to the lack of competing Auger processes, and thus the yield is quite high. In reality, there should exist a range of ionization states in the accretion disk or outflows, so the dominating ionization state of matter determines the strength of iron Kα lines and ultimately whether the lines are detectable. It is worth noting that iron absorption lines have been detected in microquasars GRS 1915+105 and GRO J1655−40 by *ASCA* (Ebisawa 1996; Ueda et al. 1998), although arguments can be made, in the case of GRO J1655−40, for the presence of an emission line, during a "dipping" period, with a characteristic profile of a disk line (see the residual plot for this case in both Ebisawa 1996 and Ueda et al. 1998). Much improved spectral capability of X-ray spectrometers on future missions, such as *Chandra*, *XMM*, and *Astro-E*, can hopefully resolve much of the ambiguity in the interpretation of emission lines observed in BHCs.

The authors gratefully acknowledge support from NASA through its Long-Term Space Astrophysics program and *RXTE* Guest Observer program. This work has made use of the results provided by the ASM/*RXTE* teams at MIT and at the *RXTE* SOF and GOF and of the archival databases maintained by the High Energy Astrophysics Science Archive Research Center at NASA's Goddard Space Flight Center.

[6] See, again, http://heasarc.gsfc.nasa.gov/docs/xte/asm_products.html for the ASM light curve.

REFERENCES

Barr, P., White, N. E., & Page, C. G. 1985, MNRAS, 216, 65
Belloni, T., Mendez, M., King, A. R., van der Klis, M., & van Paradijs, J. 1997, ApJ, 497, L145
Bromley, C. B., Chen, K., & Miller, W. A. 1997, ApJ, 475, 57
Coppi, P. S. 1999, in ASP Conf. Ser. 161, High-Energy Processes in Accreting Black Holes, ed. J. Poutanen & R. Svensson (San Francisco: ASP), 375
Cui, W., Ebisawa, K., Dotani, T., & Kubota, A. 1998, ApJ, 493, L75
Cui, W., Heindl, W. A., Rothschild, R. E., Zhang, S. N., Jahoda, K., & Focke, W. 1997a, ApJ, 474, L57
Cui, W., Heindl, W. A., Swank, J. H., Smith, D. M., Morgan, E. H., Remillard, R., & Marshall, F. E. 1997b, ApJ, 487, L73
Done, C., Mulchaey, J. S., Mushotzky, R. F., & Arnaud, K. A. 1992, ApJ, 395, 275
Ebisawa, K. 1996, in X-Ray Imaging and Spectroscopy of Cosmic Hot Plasmas, ed. F. Makino & K. Mitsuda (Tokyo: Universal Academy), 427
Ebisawa, K., Ueda, Y., Inoue, H., Tanaka, Y., & White, N. E. 1996, ApJ, 467, 419
Eikenberry, S. S., Matthews, K., Morgan, E. H., Remillard, R. A., & Nelson, R. W. 1998, ApJ, 494, L61
Esin, A. A., McClintock, J. E., & Ramesh, N. 1998, ApJ, 500, 523
Fabian, A. C., Rees, M. J., Stella, L., & White, N. E. 1989, MNRAS, 238, 729
Fender, R. P., et al. 1999, MNRAS, 304, 865
Grove, J. E., Johnson, W. N., Kroeger, R. A., McNaron-Brown, K., Skibo, J. G., & Phlips, B. F. 1998, ApJ, 500, 899
Hjellming, R. M., & Rupen, M. P. 1995, Nature, 375, 464
Hjellming, R. M., et al. 1998, ApJ, 514, 383
Jones, C., Forman, W., Tananbaum, H., & Turner, M. I. L. 1976, ApJ, 210, L9
Kitamoto, S., Takahashi, K., Yamashita, K., Tanaka, Y., & Nagase, F. 1990, PASJ, 42, 85
Kotani, T., Kawai, N., Matsuoka, M., & Brinkmann, W. 1996, PASJ, 48, 619
Kuulkers, E., Parmar, A. N., Kitamoto, S., Cominsky, L. R., & Sood, R. K. 1997, MNRAS, 291, 81
Kuulkers, E., Wijnands, R., Belloni, T., Méndez, M., van der Klis, M., & van Paradijs, J. 1998, ApJ, 494, 753
Laor, A. 1991, ApJ, 376, 90
Matt, G., Fabian, A. C., & Ross, R. R. 1996, MNRAS, 278, 1111
Mirabel, I. F., et al. 1998, A&A, 330, L9
Mirabel, I. F., & Rodríguez, L. F. 1999, ARA&A, 37, in press
Mitsuda, K., et al. 1984, PASJ, 36, 741
Oosterbroek, T., Parmar, A. N., Kuulkers, E., Belloni, T., van der Klis, M., Frontera, F., & Santangelo, A. 1998, A&A, 340, 431
Parmar, A. N., Angelini, L., & White, N. E. 1995, ApJ, 452, L129
Parmar, A. N., Stella, L., & White, N. E. 1986, ApJ, 304, 664
Parmar, A. N., Williams, O. R., Kuulkers, E., Angelini, L., & White, N. E. 1997, A&A, 319, 855
Priedhorsky, W. C. 1986, Ap&SS, 126, 89
Ross, R. R., & Fabian, A. C. 1993, MNRAS, 261, 74
Tanaka, Y., & Lewin, W. H. G. 1995, in X-Ray Binaries, ed. W. H. G. Lewin, J. van Paradijs, & E. P. J. van den Heuvel (Cambridge: Cambridge Univ. Press), 126
Tomsick, J. A., Lapshov, L., & Kaaret, P. 1998, ApJ, 494, 747
Ueda, Y., Inoue, H., Tanaka, Y., Ebisawa, K., Nagase, F., Kotani, T., & Gehrels, N. 1998, ApJ, 492, 782
Życki, P. T., Done, C., & Smith, D. A. 1999, MNRAS, 305, 231